Chapter 3

CHAPTER 3

PREPARATION AND CHARACTERIZATION OF QUATERNARY SEMICONDUCTOR Cu_2NiSnS_4 (CNTS) NANOPARTICLES - POTENTIAL SOLAR ABSORBER MATERIALS

Chapter three deals with the synthesis of Cu_2NiSnS_4 nanoparticles by a facile chemical route method. The structural, morphological, optical and electrical characteristics of the synthesized nanoparticles have been analyzed. This chapter deals with the optimization of the CNTS composition concentration for application as solar absorber materials.

3.1 INTRODUCTION

Copper (Cu) based chalcogenides such as $Cu(In,Ga)(S,Se)_2$ (CIGS/Se) and (CdTe) are promising light absorber materials. However, the lack of availability, extreme toxicity of the constituent elements, and the need for expensive precursor materials prevent the large scale production of thin film photovoltaic cells. It is important to develop low cost, naturally abundant, non-toxic and environment friendly chalcogenide materials for photovoltaic applications. In recent years, chalcopyrite quaternary semiconductors such as $Cu_2ZnSnSe_4$ (CZTSe) and Cu_2ZnSnS_4(CZTS) have attracted much attention due to their optimum optical band gap values (~1.5 eV) and high absorption coefficients (~10^4 cm^{-1}) for potential application in thin film photovoltaic cells. In addition, Cu_2NiSnS_4 (CNTS) is also considered as an alternative for Cu_2ZnSnS_4 (CZTS) because of its suitable band gap around 1.1-1.5 eV and large absorption coefficient of ~10^4 cm^{-1} [1-4]. In earlier investigations, CZTS and CNTS thin films and nanoparticles have been synthesized by using different synthesis methods such as the spray sandwich method [4], direct solution dip coating [2,3], electro deposition [5,6], facile solvothermal method [8], hydrothermal method [1,7] and facile chemical route method [9]. The chemical precipitation method of synthesis of CNTS nanoparticles has attracted much attention due to its ease of operation, low cost and controllability of the components. In this study, the structure, composition, morphology, optical properties and stoichiometry of CNTS particles synthesized by the chemical route have been investigated.

3.2 EXPERIMENTAL DETAILS

3.2.1 Materials

The precursor materials copper chloride (99.9 % pure, $CuCl_2.2H_2O$), nickel chloride (99.9 % pure, $NiCl_2.6H_2O$), stannous chloride (99.9 % pure, ($SnCl_2.2H_2O$), and thiourea (99.9 % pure, CH_4N_2S) were procured from Sigma Aldrich chemicals. All the chemicals were of analytical grade and used as received without further purification.

3.2.2 Synthesis procedure and characterization techniques

The metallic precursor solution for the synthesis of Cu_2SnS_4 (CTS) nanoparticles was prepared from 2 mmol of copper chloride, 0.8 mmol of stannous chloride and 4 mmol of thiourea. The CNTS nanoparticles were prepared by incorporating the CTS nanoparticles with Ni content (adding 0.2 mmol of nickel chloride) to obtain CNTS nanoparticles. The compounds were added in sequence allowing sufficient time to dissolve the solutes and the pH was maintained at 8 by adding a few drops of diluted ammonia to the aqueous solution. The solutions were stirred for 4 h at a constant temperature of 90 °C. After continuous and uniform stirring, the solutions were kept at room temperature for several hours to allow the precipitate to settle down. The precipitate was collected and washed with water and ethanol several times to remove the impurities present in the solution. Finally, the obtained product was dried at 90 °C for 4 h to attain purity of phase and more crystallite nature of the CTS and CNTS nanoparticles.

The phase structures of the CTS and CNTS nanoparticles were identified by recording X-ray diffraction spectra in the 2θ range 20 ° - 80 ° using Rigaku X-ray diffractometer with CuKα radiation (λ= 1.5406 Å) source. The UV–Vis–NIR spectrum (DRS mode) was obtained using Jasco V-570 UV–Vis–NIR spectrophotometer. The chemical compositions were analyzed by Energy dispersive X-ray spectroscopy (EDAX analyser-Bruker-4010) along with scanning electron microscopy (SEM - Hitachi equipment).

3.3 RESULTS AND DISCUSSION

3.3.1 Structural property

The XRD patterns of the synthesized CTS nanoparticles are shown in Figure 3.1(a). The major XRD diffraction peaks appeared at 2θ =28.1, 33.04, 47.15 and 56.4 ° corresponding to (111), (200), (220), and (312) planes respectively. The prepared CTS nanoparticles belong to cubic structure in the space group F-43m (JCPDS card no: 089-4714; 27-0198). The minor impurity peaks at 54.45 ° are attributed to the (414) planes of Sn_2S_3. Figure 3.1(b) shows the XRD patterns of CNTS nanoparticles. The major diffraction peaks appeared at 2θ =28.56, 33.4, 47.15 and 56.18 corresponding to (111), (200), (220) and (311) planes respectively of the cubic structure [1, 2]. Addition of Ni to CTS nanoparticles did not alter their cubic structure. The Ni atoms are incorporated into the cubic structure of CTS nanoparticles leading to the formation of CNTS nanoparticles. This is well matched with the space group F-43m (JCPDS card no: 26-0552). No other impurity peaks are observed for the CNTS nanoparticles.

The lattice parameter and crystallite size were calculated using the Bragg's equation,

$$n\lambda = 2d_{hkl}sin\theta \tag{3.1}$$

Where n is a positive integer, λ is the radiation wavelength, d_{hkl} is the inter-planar distance corresponding to the h, k and l Miller indices and θ is the Bragg's angle of the (hkl) planes. The Inter-planer spacing for cubic structure is

$$d_{hkl} = \frac{a}{\sqrt{(h^2+k^2+l^2}} \tag{3.2}$$

The lattice parameter (a) calculated from the refined pattern is a = 5.432 Å, which is in good agreement with the standard values (JCPDS card number mentioned above). The average crystallite size was calculated employing the Scherrer formula,

$$D = \frac{k\lambda}{\beta cos\theta} \tag{3.3}$$

Where k is the shape factor (k= 0.9), λ is the wavelength (1.5406 Å) of the X-ray used, β is the full width at half maximum (FWHM) and θ is the Bragg diffraction angle.

The average crystallite size (D) of CNTS nanoparticles was found to be 10.9 nm from the most prominent (111) plane peak [4].

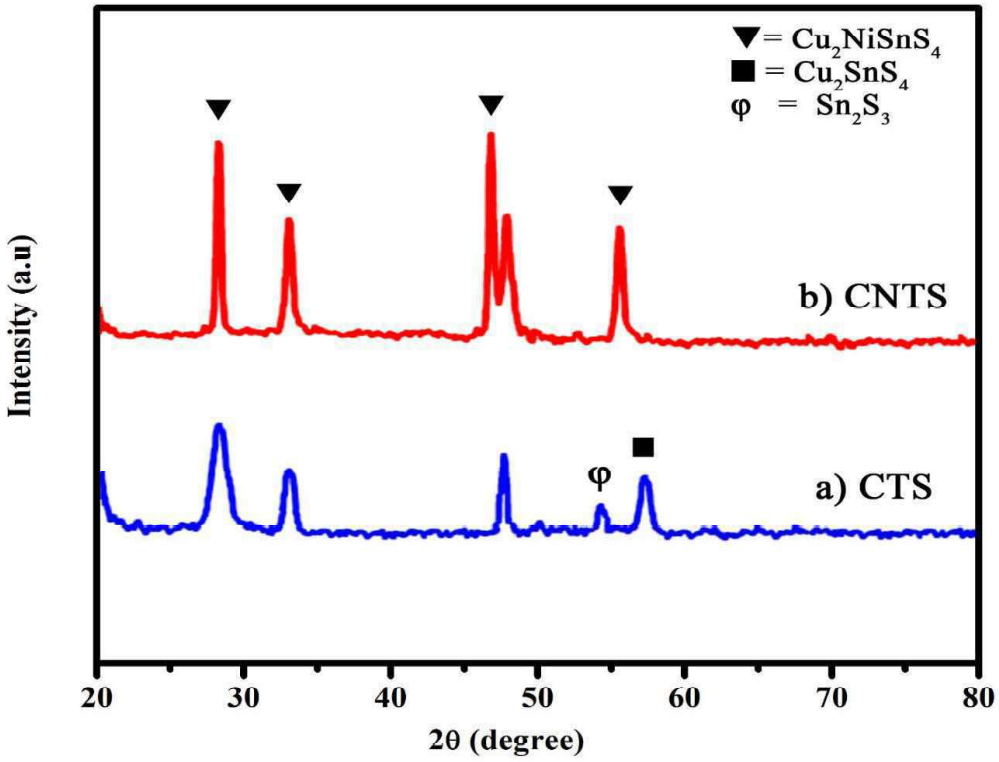

Figure 3.1 X-ray diffraction patterns of (a) CTS and (b) CNTS

3.3.2 Optical analysis

The optical absorption spectra of the CTS and CNTS nanoparticles recorded in the wavelength range of 250-900 nm (UV-1700 series) are shown in Figure 3.2(a) and 3.2(b). The optical band gap is calculated by using the Tauc relation [10].

$$(\alpha h\nu)^n = A(h\nu - E_g) \tag{3.4}$$

$$\alpha = \frac{A(h\nu - E_g)^{1/n}}{h\nu} \tag{3.5}$$

Where, h is the Planck constant, ν is the frequency, A is the absorbance and Eg is the optical band gap. The exponent n is 1/2 for direct band gap and 2 for indirect band gap transition. From earlier literature, CTS and CNTS nanoparticles are direct band gap semiconductors [6, 8 and 10]. Figure 3.2(c) and 3.2(d) show the plot of $(\alpha h\nu)^2$ versus hν for the CTS and CNTS nanoparticles. The linear nature of the plots confirms the direct

transition. The tangents to these curves, when extrapolated to zero, give the band gap values as 1.18 eV and 1.31 eV respectively for the CTS and CTS nanoparticles. These results are in good agreement with values reported in the literature [8].

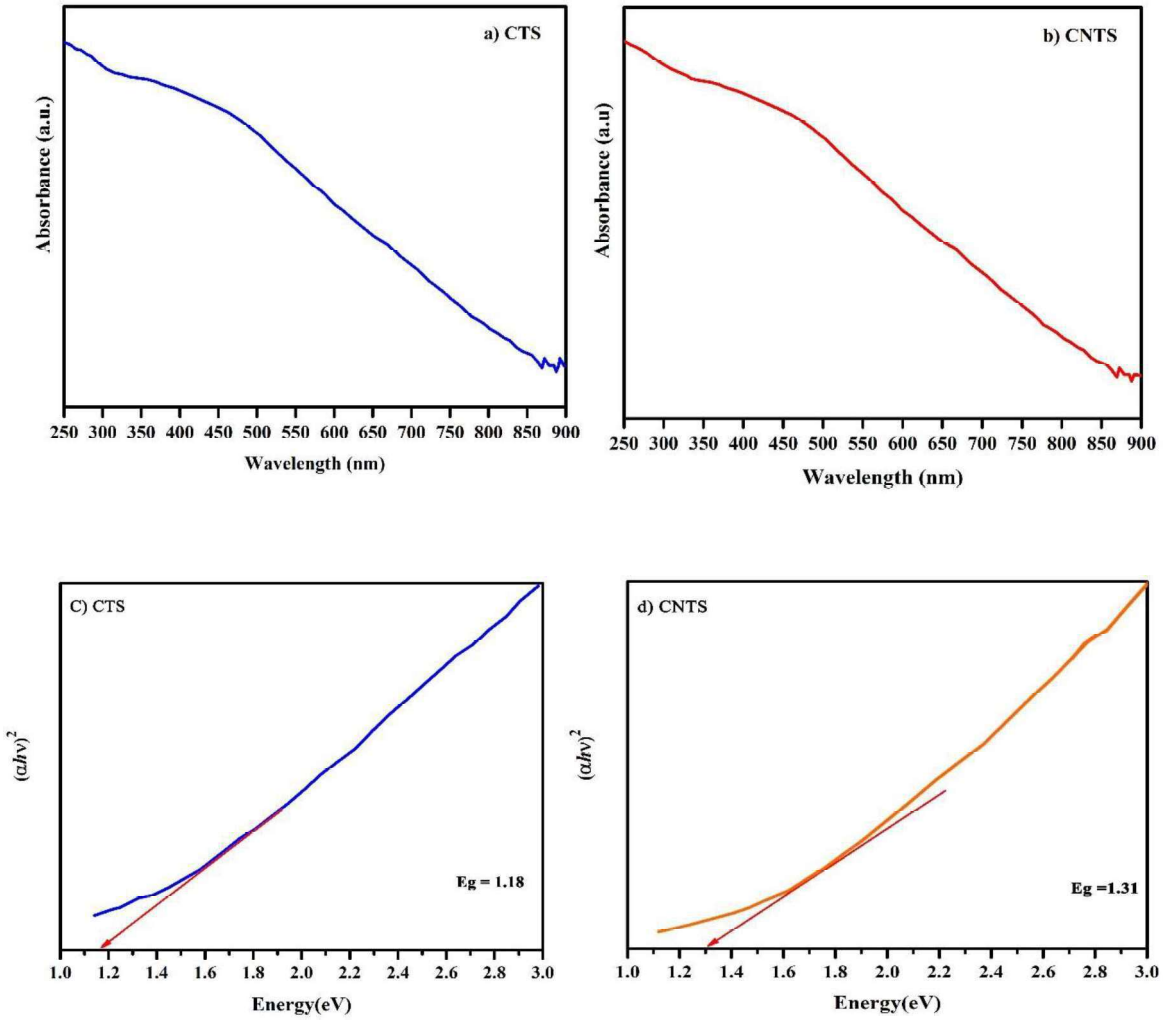

Figure 3.2 Absorption spectra of (a) CTS and (b) CNTS and Optical energy band gap of (c) CTS and (d) CNTS nanoparticles

3.3.3 Morphological analysis

Figure 3.3 (a) and 3.3(b) show the scanning electron microscope images of CTS and CNTS nanoparticles synthesized by the facile chemical route method. The CTS and CNTS nanoparticles are both observed to be densely packed, forming clusters with flake like morphology.

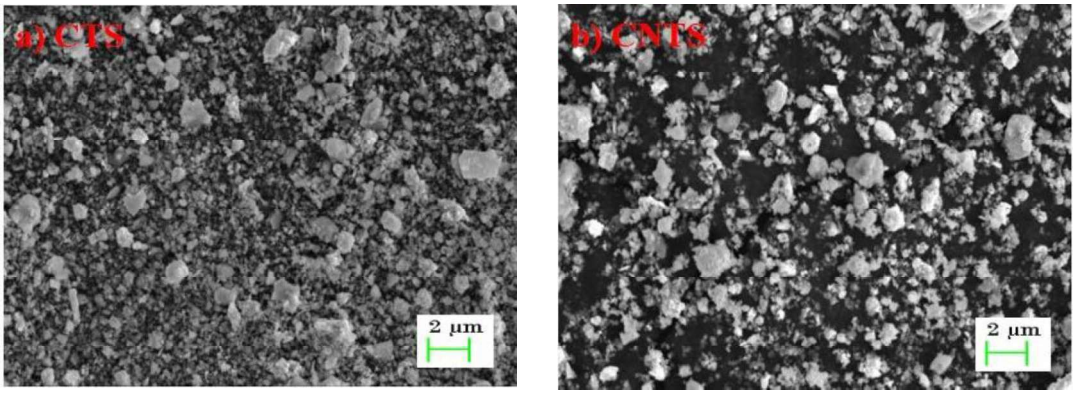

Figure 3.3. SEM images of (a) CTS (b) CNTS nanoparticles

3.3.4 Energy dispersive X-ray spectroscopy analysis

The chemical compositions of the CTS and CNTS nanoparticles were obtained from the EDAX spectra shown in Figure 3.4(a) and 3.4(b). The obtained elemental ratios of Cu:Sn:S (2.10:1.08:3.80) and Cu:Ni:Sn:S (2.00:0.85:0.90:3.89), indicate that the stoichiometric ratios are in very good agreement with the theoretical values of 2:1:4 and 2:1:1:4 for CTS and CNTS nanoparticles respectively.

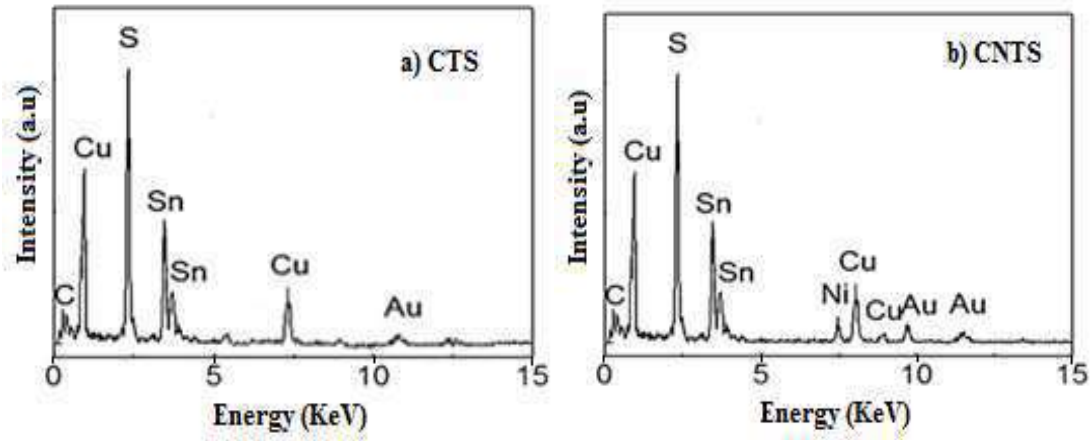

Figure 3. 4 EDAX spectra of (a) CTS and (b) CNTS nanoparticles

3.3.5 Cyclic voltammetry

The electrochemical studies were carried out using the three electrode system with 0.1 M of phosphate buffer solution (PBS) electrolyte. The cyclic voltammetric (CV) measurements were carried out in the potential range of -1.0 V to 1.0 V with respect to an Ag/AgCl reference electrode. Platinum wire and glassy carbon served as the counter and working electrodes respectively. The electrochemical behavior for the prepared CTS and CNTS nanoparticles was measured with a scan rate of 20 mVs^{-1}. Earlier investigators [11] have studied the reduction behaviors of Cu, Sn, and Zn from a unitary system. The complex agent trisodium citrate was used to reduce the variations in the reduction potentials of each material. The reduction potential was lowered from -0.2 V (vs. Ag/AgCl) to -0.5 V for Cu, -0.5 V (vs. Ag/AgCl) to -0.7 V for Sn, and -1.2 V (vs. Ag/AgCl) to -0.7 V for Zn. CZTS thin film has been reported to be a better alternative to replace the expensive platinum (Pt) counter electrode (CE) in DSSCs [12]. Ghosh et al [13] have shown that the reduction peak current density of CNTS is higher than that of CFTS (Cu_2FeSnS_4) and CCTS (Cu_2CoSnS_4) thin film electrodes.

In the present study, CTS nanoparticles exhibit oxidation and reduction peaks at the potentials of 0.51 V and -0.74 V respectively as observed in Figure 3.5(a). On incorporating the CTS nanoparticles with Ni content (nickel chloride), the resultant CNTS nanoparticles exhibit strong oxidation and reduction peaks at the potentials of 0.48 V and -0.53 V respectively, as shown in Figure 3.5(b). The maximum reduction peak current density values for CTS and CNTS nanoparticles are -0.0084 mA/cm^2 and -0.0113 mA/cm^2 respectively. The reduction peak current density for CNTS is observed to be higher than that for CTS. According to earlier researchers, electrocatalytic performance depends on the specific surface area, morphology and elemental composition of quaternary chalcopyrite sulphides [13]. The CV curves in Figure 3.5 show better superior catalytic activity of CNTS nanoparticles when compared to CTS nanoparticles which may be attributed to the change in the elemental composition due to the incorporation of Ni content.

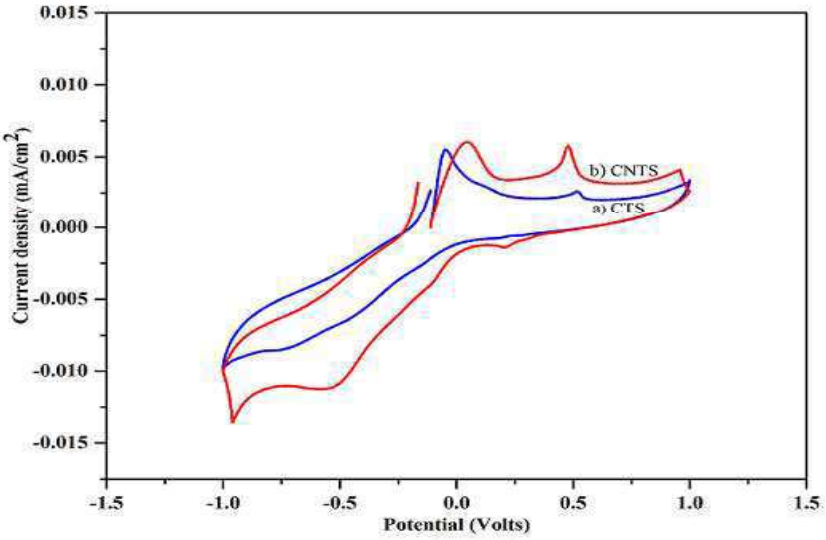

Figure 3.5 CV curve of CTS and CNTS nanoparticles

3.4 CONCLUSION

Quaternary semiconductor CNTS nanoparticles have been synthesized by the facile chemical route method. The phase-pure cubic crystal structure of the synthesized nanoparticles has been confirmed by XRD analysis. SEM images show that the prepared nanoparticles are densely packed, forming clusters with flake-like morphology. Well controlled stoichiometry with the perfect elemental ratio is observed for the prepared nanoparticles by EDAX. The electrochemical studies were carried out by cyclic voltammetric (CV) measurements in the potential range of -1.0 V to +1.0 V. The CV curves shows better superior catalytic activity of CNTS nanoparticles when compared to CTS nanoparticles which may be attributed to the change in the elemental composition due to the incorporation of Ni content. The observed increase in optical band gap values from 1.18 eV for CTS nanoparticles to 1.31 eV for CNTS nanoparticles indicates that CNTS nanoparticles show better performance as potential absorber materials for thin-film photovoltaic applications.

REFERENCES

1. Babu, G. S. D., Shajan, X. S., Alwin, S., Ramasubbu, V., & Balerao, G. M. (2018). Effect of reaction period on stoichiometry, phase purity, and morphology of hydrothermally synthesized Cu_2NiSnS_4 Nanopowder. Journal of Electronic Materials, 47, 312-322.

2. Jariwala, A., Chaudhuri, T. K., Patel, S., Toshniwal, A., Kheraj, V., & Ray, A. (2018). Direct-coated copper nickel tin sulphide (Cu_2NiSnS_4) thin films from molecular ink. Materials Letters, 215, 118-120.

3. Mokurala, K., Mallick, S., Bhargava, P., Siol, S., Klein, T. R., & Van Hest, M. F. (2017). Influence of dipping cycles on physical, optical, and electrical properties of Cu_2NiSnS_4: direct solution dip coating for photovoltaic applications. Journal of Alloys and Compounds, 725, 510-518.

4. Dridi, S., Bitri, N., & Abaab, M. (2017). Synthesis of quaternary Cu_2NiSnS_4 thin films as a solar energy material prepared through «Spray» technique. Materials Letters, 204, 61-64.

5. Chen, H. J., Fu, S. W., Tsai, T. C., & Shih, C. F. (2016). Quaternary Cu_2NiSnS_4 thin films as a solar material prepared through electrodeposition. Materials Letters, 166, 215-218.

6. Yang, C. L., Chen, Y. H., Lin, M., Wu, S. L., Li, L., Liu, W. C., ... & Zhang, F. M. (2016). Structural, optical and magnetic properties of Cu_2NiSnS_4 thin films deposited by facile one-step electrodeposition. Materials Letters, 166, 101-104.

7. Wang, T. X., Li, Y. G., Liu, H. R., Li, H., & Chen, S. X. (2014). Flower-like Cu_2NiSnS_4 nanoparticles synthesized by a facile solvothermal method. Materials Letters, 124, 148-150.

8. Sarkar, S., Das, B., Midya, P. R., Das, G. C., & Chattopadhyay, K. K. (2015). Optical and thermoelectric properties of chalcogenide based Cu_2NiSnS_4 nanoparticles synthesized by a novel hydrothermal route. Materials Letters, 152, 155-158.

9. Lydia, R., & Sreedhara Reddy, P. (2013). Effect of pH on the characteristics of Cu_2ZnSnS_4 nanoparticles. International Scholarly Research Notices, 2013.

10. Shelke, H. D., Lokhande, A. C., Kim, J. H., & Lokhande, C. D. (2017). Photoelectrochemical (PEC) studies on Cu_2SnS_3 (CTS) thin films deposited by chemical bath deposition method. Journal of colloid and interface science, 506, 144-153.

11. Shin, S., Park, C., Kim, C., Kim, Y., Park, S., & Lee, J. H. (2016). Cyclic voltammetry studies of copper, tin and zinc electrodeposition in a citrate complex system for CZTS solar cell application. Current Applied Physics, 16(2), 207-210.

12. Chen, S., Xu, A., Tao, J., Tao, H., Shen, Y., Zhu, L., ... & Pan, L. (2015). In-situ and green method to prepare Pt-free Cu_2ZnSnS_4 (CZTS) counter electrodes for efficient and low cost dye-sensitized solar cells. ACS Sustainable Chemistry & Engineering, 3(11), 2652-2659.

13. Ghosh, A., Biswas, A., Thangavel, R., & Udayabhanu, G. (2016). Photo-electrochemical properties and electronic band structure of kesterite copper chalcogenide Cu_2–II–Sn–S_4 (II= Fe, Co, Ni) thin films. RSC Advances, 6(98), 96025-96034.